Lattice QCD Calculation of the Two-Photon Exchange Contribution to the Muonic-Hydrogen Lamb Shift

Yang Fu,[1] Xu Feng,[1,2,3,*] Lu-Chang Jin,[4,5,†] and Chen-Fei Lu[1]
[1]*School of Physics, Peking University, Beijing 100871, China*
[2]*Collaborative Innovation Center of Quantum Matter, Beijing 100871, China*
[3]*Center for High Energy Physics, Peking University, Beijing 100871, China*
[4]*Department of Physics, University of Connecticut, Storrs, Connecticut 06269, USA*
[5]*RIKEN-BNL Research Center, Brookhaven National Laboratory, Building 510, Upton, New York 11973, USA*

(Received 3 February 2022; accepted 11 April 2022; published 29 April 2022)

We develop a method for lattice QCD calculation of the two-photon exchange contribution to the muonic-hydrogen Lamb shift. To demonstrate its feasibility, we present the first lattice calculation with a gauge ensemble at $m_\pi = 142$ MeV. By adopting the infinite-volume reconstruction method along with an optimized subtraction scheme, we obtain with statistical uncertainty $\Delta E_{\mathrm{TPE}} = -28.9(4.9)\ \mu\mathrm{eV} + 93.72\ \mu\mathrm{eV/fm}^2 \cdot \langle r_p^2 \rangle$, or $\Delta E_{\mathrm{TPE}} = 37.4(4.9)\ \mu\mathrm{eV}$, which is consistent with the previous theoretical results in a range of 20–50 μeV.

DOI: 10.1103/PhysRevLett.128.172002

Introduction.—Lamb shift is an important observable, whose discovery laid the foundation for the modern quantum electrodynamics. A decade ago, measurements of muonic-hydrogen (μH) Lamb shift [1,2] yielded the most precise determination of the proton charge radius $\langle r_p^2 \rangle$, but raised a 7σ discrepancy from the CODATA-2010 value [3], known as the proton radius puzzle. In 2019, two experiments reported results which agree with the μH measurements [4,5] and represented a decisive step towards solving the puzzle. In the theoretical understanding of both spectroscopy and scattering, the two-photon exchange (TPE) contribution is of special interest. It introduces the largest theoretical uncertainty in extracting $\langle r_p^2 \rangle$ from the μH Lamb shift [6] and plays an important role in resolving the proton electric to magnetic form factor ratio puzzle [7].

Several approaches have been proposed to calculate the TPE correction to the μH Lamb shift [8–19], where the correction is usually divided into Born and non-Born pieces. The former is well constrained by the experimental data, while the latter contains a subtraction function, which is poorly constrained and relies on model, thus leading to a large systematic uncertainty. It was proposed recently that the subtraction function can be further constrained by the dilepton electroproduction [20]. To date, the theoretical results of the TPE correction ΔE_{TPE} are summarized in Fig. 1. These results are rather consistent but still vary in a range of 20–50 μeV.

The total $2S - 2P$ Lamb shift is given by [6]

$$\Delta E_{\mathrm{LS}}^{\mathrm{theory}} = 206033.6(1.5) - 5227.5(1.0)\langle r_p^2 \rangle + \Delta E_{\mathrm{TPE}}. \tag{1}$$

In Eq. (1) and through out the Letter we assume radii to be in fm, resulting energies in μeV. Using $\Delta E_{\mathrm{TPE}} = 33.2(2.0)\ \mu$eV from Ref. [16] and the experimental value $\Delta E_{\mathrm{LS}}^{\mathrm{exp}} = 202370.6(2.3)\ \mu$eV, one obtains $\sqrt{\langle r_p^2 \rangle} = 0.84087(39)$ fm, which causes the radius puzzle [2] compared to the CODATA-2010 value $\sqrt{\langle r_p^2 \rangle} = 0.8775(51)$ fm [3]. To resolve the puzzle, ΔE_{TPE} is

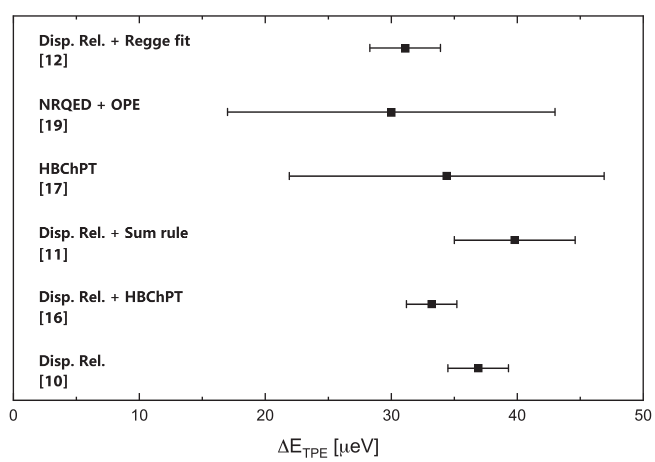

FIG. 1. Theoretical results for ΔE_{TPE}. From top to bottom, the results are referred to Refs. [10–12,16,17,19], respectively.

required to be $\sim$300 μeV, 10 times larger than the current theoretical results. Although $\Delta E_{\rm TPE}$ is unlikely responsible for such a large discrepancy, it causes the largest theoretical uncertainty in the determination of $\langle r_p^2\rangle$. More refined $\langle r_p^2\rangle$ would inevitably require an improved determination of $\Delta E_{\rm TPE}$, particularly from lattice QCD to avoid the uncertainties induced by model assumptions.

In this Letter, we develop a lattice QCD method to calculate $\Delta E_{\rm TPE}$ and perform a realistic calculation at the pion mass $m_\pi = 142$ MeV.

Two-photon exchange contribution.—We start with the spin-averaged forward doubly virtual Compton scattering tensor defined in Euclidean space,

$$\begin{aligned}\mathcal{T}_{\mu\nu}(P,Q) &= \frac{1}{8\pi M}\int d^4x e^{iQ\cdot x}\langle p|T[J_\mu(x)J_\nu(0)]|p\rangle \\ &= \left(-\delta_{\mu\nu}+\frac{Q_\mu Q_\nu}{Q^2}\right)\mathcal{T}_1(\nu,Q^2) \\ &\quad -\left(P_\mu-\frac{P\cdot Q}{Q^2}Q_\mu\right)\left(P_\nu-\frac{P\cdot Q}{Q^2}Q_\nu\right) \\ &\quad \times\frac{\mathcal{T}_2(\nu,Q^2)}{M^2},\end{aligned} \tag{2}$$

where $\nu = P\cdot Q/M$ with $P = (iM,\mathbf{0})$ and $Q = (Q_0,\mathbf{Q})$ the Euclidean proton and photon four-momenta. M is the proton mass, $J_{\mu,\nu}$ are the electromagnetic quark currents, and $\mathcal{T}_{1,2}$ are the Lorentz scalar functions.

The relative energy shift to the nS state is given by [8]

$$\begin{aligned}E &= \frac{8m\alpha^2}{\pi}|\phi_n(0)|^2\int d^4Q \\ &\quad\times\frac{(Q^2+2Q_0^2)\mathcal{T}_1(iQ_0,Q^2)-(Q^2-Q_0^2)\mathcal{T}_2(iQ_0,Q^2)}{Q^4(Q^4+4m^2Q_0^2)},\end{aligned} \tag{3}$$

with m the lepton mass and $|\phi_n(0)|^2$ the square of the nS-state wave function at the origin, known from literature, e.g., Ref. [10]. Note that the nP-state wave function vanishes at the origin, hence it does not receive any corrections from TPE at this order.

The TPE correction to the μH Lamb shift has no infrared (ir) divergence because the binding energy serves as an ir regulator. By treating the proton as a pointlike particle with the corrections from $\langle r_p^2\rangle$, one can calculate such contribution using bound-state QED [8,21,22]. However, more precise comparison between theory and experiment is limited due to ignorance of the proton structure. The energy shift E defined in Eq. (3) contains all the required structure information, but is unfortunately ir divergent as the lepton in the Compton scattering is not bounded. Here, the idea is to obtain the structure-dependent TPE correction from Eq. (3) by subtracting the contributions from a pointlike proton and the third Zemach moment [10]. The former is described by pointlike scalar functions

$$\mathcal{T}_1^{pt} = \frac{M}{\pi}\frac{\nu^2}{Q^4-4M^2\nu^2},\qquad \mathcal{T}_2^{pt} = \frac{M}{\pi}\frac{Q^2}{Q^4-4M^2\nu^2}, \tag{4}$$

and the latter is given by

$$E^Z = \alpha^2|\phi_n(0)|^2\int\frac{dQ^2}{Q^2}\frac{8mM}{3(M+m)Q}\langle r_p^2\rangle. \tag{5}$$

After the subtraction of E^{pt} and E^Z, one obtains the ir-finite TPE contribution $\Delta E = E - E^{pt} - E^Z$. The desired $\Delta E_{\rm TPE}$ shown in Eq. (1) is defined as the difference between energy shifts to the nP and nS states and thus we have $\Delta E_{\rm TPE} = -\Delta E$.

In a realistic lattice QCD calculation, the first difficulty to conquer is to write $\Delta E_{\rm TPE}$ in terms of the hadronic functions calculable via lattice simulations and maintain the ir cancellation automatically.

Lattice QCD methodology.—On the lattice, we prefer to rewrite Eq. (3) in terms of $T_1 = \mathcal{T}_{00}$ and $T_2 = \sum_i \mathcal{T}_{ii}$ as

$$E = -16m\alpha^2|\phi_n(0)|^2\int_\varepsilon\frac{dQ^2}{Q^4}\int_{-\frac{\pi}{2}}^{\frac{\pi}{2}}d\theta(\alpha_1T_1+\alpha_2T_2), \tag{6}$$

with

$$\alpha_1(Q) = \frac{1-\sin^4\theta}{1+\sin^2\theta/\tau_\ell},\qquad \alpha_2(Q) = \frac{\sin^2\theta\cos^2\theta}{1+\sin^2\theta/\tau_\ell},$$
$$\tau_\ell = \frac{Q^2}{4m^2}. \tag{7}$$

Here the angle θ is defined as $Q_0 = Q\sin\theta$ and $|\mathbf{Q}| = Q\cos\theta$. The notation $\int_\varepsilon$ indicates that the integral is performed in the region of $Q^2\geq\varepsilon^2$ with an ir regulator ε.

Combining Eqs. (2) and (6) yields

$$E = \frac{2m\alpha^2}{\pi M}|\phi_n(0)|^2\sum_{i=1,2}\int d^4x\bar{\omega}_i(\mathbf{x},t)H_i(\mathbf{x},t), \tag{8}$$

where the hadronic functions are defined as

$$\begin{aligned}H_1(\mathbf{x},t) &= \langle p|T[J_0(\mathbf{x},t)J_0(0)]|p\rangle,\\ H_2(\mathbf{x},t) &= \langle p|T[\mathbf{J}(\mathbf{x},t)\cdot\mathbf{J}(0)]|p\rangle.\end{aligned} \tag{9}$$

The weight functions $\bar{\omega}_i(\mathbf{x},t)$ are given by

$$\bar{\omega}_i(\mathbf{x},t) = -\int_\varepsilon\frac{dQ^2}{Q^4}\int_{-\frac{\pi}{2}}^{\frac{\pi}{2}}d\theta\alpha_i(Q)f(Q;x) \tag{10}$$

with

$$f(Q;x) = \cos(Q_0t)j_0(|\mathbf{Q}||\mathbf{x}|). \tag{11}$$

Here an average over the spatial directions is taken and $j_n(x)$ are the spherical Bessel functions.

Using the infinite-volume reconstruction method [23], we split the time integral in Eq. (8) into the regions $|t| < t_s$ and $|t| \geq t_s$, and have

$$E = E^{<t_s} + E^{\geq t_s}. \tag{12}$$

Both ground state, i.e., proton, and excited states such as the Δ resonance, $p + \pi$, and $p + 2\pi$ can contribute to E. At sufficiently large t_s, ground-state dominance allows us to relate $H_i(\mathbf{x}, t)$ at $|t| \geq t_s$ to $H_i(\mathbf{x}, t_s)$. Thus, $E^{\geq t_s}$ can be written as

$$E^{\geq t_s} = \frac{2m\alpha^2}{\pi M}|\phi_n(0)|^2 \sum_{i=1,2} \int d^3\mathbf{x} \bar{L}_i(\mathbf{x}, t_s) H_i(\mathbf{x}, t_s), \tag{13}$$

where the weight function $\bar{L}_i$ is defined as

$$\bar{L}_i(\mathbf{x}, t_s) = -\int_\varepsilon \frac{dQ^2}{Q^4} \int_{-\frac{\pi}{2}}^{\frac{\pi}{2}} d\theta \alpha_i(Q) g(Q; \mathbf{x}, t_s) \tag{14}$$

with

$$g(Q; \mathbf{x}, t_s) = 2\int_{t_s}^{\infty} dt f(Q; x) e^{-(\sqrt{M^2+\mathbf{Q}^2}-M)(t-t_s)}. \tag{15}$$

We originally hope that the ir divergent part is isolated by $E^{\geq t_s}$ and thus only the weight function $\bar{L}_i$ is divergent when $\varepsilon \to 0$. However, the situation is more complicated than expected as $E^{<t_s}$ is also ir divergent. [Although associated with $H_i(\mathbf{x}, t)$ at small t, $\bar{\omega}_i$ receives significant long-distance contributions from the leptonic part and thus is ir singular.] To solve this difficulty, we split the weight functions into two parts:

$$\bar{\omega}_i = \hat{\omega}_i + \delta\omega_i, \qquad \bar{L}_i = \hat{L}_i + \delta L_i, \tag{16}$$

where the divergent part is absorbed by $\delta\omega_i$ and δL_i with

$$\delta\omega_i = -\int_\varepsilon \frac{dQ^2}{Q^4} \int_{-\frac{\pi}{2}}^{\frac{\pi}{2}} d\theta \alpha_i(Q),$$
$$\delta L_i = -\int_\varepsilon \frac{dQ^2}{Q^4} \int_{-\frac{\pi}{2}}^{\frac{\pi}{2}} d\theta \alpha_i(Q) g_0(Q; \mathbf{x}, t_s), \tag{17}$$

and

$$g_0(Q; \mathbf{x}, t_s) = \frac{1}{M} \frac{\cos^2\theta}{\tau_p + \sin^2\theta} - 2t_s, \qquad \tau_p = \frac{Q^2}{4M^2}. \tag{18}$$

One can confirm that $\hat{\omega}_i$ and $\hat{L}_i$ are now ir finite. Accordingly, the energies $E^{<t_s}$ and $E^{\geq t_s}$ are written as

$$E^{<t_s} = \hat{E}^{<t_s} + \delta E^{<t_s}, \qquad E^{\geq t_s} = \hat{E}^{\geq t_s} + \delta E^{\geq t_s}. \tag{19}$$

Through the low-momentum expansion of $T_i(Q)$ [24], we obtain for the large t_s

$$K_i \equiv \frac{1}{2M} \int_{-t_s}^{t_s} dt \int d^3\mathbf{x} H_i(\mathbf{x}, t) = \begin{cases} 2t_s, & i = 1, \\ \frac{3}{M}, & i = 2. \end{cases} \tag{20}$$

This relation allows us to rewrite $\delta E^{<t_s}$ in a structure-independent form

$$\delta E^{<t_s} = -\frac{4m\alpha^2}{\pi}|\phi_n(0)|^2 \sum_{i=1,2} \int_\varepsilon \frac{dQ^2}{Q^4} \int_{-\frac{\pi}{2}}^{\frac{\pi}{2}} d\theta \alpha_i(Q) K_i. \tag{21}$$

The last step is to perform the subtraction of $\Delta E = E - E^{pt} - E^Z$ as mentioned earlier. Here E^{pt} can be calculated using the pointlike proton contributions

$$T_1^{pt} = \frac{M}{\pi} \frac{Q^2 - Q_0^2}{Q^4 + 4M^2 Q_0^2}, \qquad T_2^{pt} = \frac{M}{\pi} \frac{3Q_0^2}{Q^4 + 4M^2 Q_0^2}. \tag{22}$$

The same ir regulator ε shall be introduced to make E^{pt} and E^Z finite. One can relate 1 and $\langle r_p^2 \rangle$ to $H_1(\mathbf{x}, t_s)$ as [25]

$$1 = \int d^3\mathbf{x} L_0(\mathbf{x}, t_s) H_1(\mathbf{x}, t_s),$$
$$\langle r_p^2 \rangle = \int d^3\mathbf{x} L_r(\mathbf{x}, t_s) H_1(\mathbf{x}, t_s), \tag{23}$$

with t_s sufficiently large for ground-state dominance and

$$L_0(\mathbf{x}, t_s) = \frac{1}{2M}, \qquad L_r(\mathbf{x}, t_s) = \frac{1}{4M}\left(\mathbf{x}^2 - \frac{3 + 6Mt_s}{2M^2}\right). \tag{24}$$

These relations allow us to write E^{pt} and E^Z as an integral of $H_1(\mathbf{x}, t_s)$. Finally, we obtain

$$\Delta E = \frac{2m\alpha^2}{\pi M}|\phi_n(0)|^2 \Bigg\{ \sum_{i=1,2} \bigg[\int_{-t_s}^{t_s} d^4x \omega_i(\mathbf{x}, t) H_i(\mathbf{x}, t) + \int d^3\mathbf{x} L_i(\mathbf{x}, t_s) H_i(\mathbf{x}, t_s) \bigg] - 2M \int_\varepsilon \frac{dQ^2}{Q^4} \int d\theta \alpha_2(Q)(K_2 - 4\pi T_2^{pt}) \Bigg\}. \tag{25}$$

Although the weight functions $\bar{\omega}_i$, $\hat{\omega}_i$, $\bar{L}_i$, and $\hat{L}_i$ are introduced in the intermediate steps, in the master formula (25) ω_i and L_i are used instead. ω_i for $i = 1, 2$, and L_2 can be directly related to the ir-finite ones $\hat{\omega}_i$ and $\hat{L}_2$ as $\omega_i(\mathbf{x}, t) = \hat{\omega}_i(\mathbf{x}, t)$, $L_2(\mathbf{x}, t_s) = \hat{L}_2(\mathbf{x}, t_s)$. The subtlety appears in L_1. Since the subtraction E^Z appears only in terms of H_1 and not H_2, thus L_1 is now a linear combination of $\hat{L}_1$ and L_r as

$$
\begin{aligned}
L_1(\mathbf{x},t_s) &= \hat{L}_1(\mathbf{x},t_s) - \int_\varepsilon \frac{dQ^2}{Q^2}\frac{4\pi M^2}{3(M+m)Q}L_r(\mathbf{x},t_s) \\
&= -\int_\varepsilon \frac{dQ^2}{Q^4}\left\{\int_{-\frac{\pi}{2}}^{\frac{\pi}{2}} d\theta\alpha_1(Q)[g-g_0](Q;\mathbf{x},t_s)\right. \\
&\quad \left. + \frac{4\pi M^2 Q}{3(M+m)}L_r(\mathbf{x},t_s)\right\}. \qquad (26)
\end{aligned}
$$

After the ir cancellation, the limit $\varepsilon \to 0$ can be taken for Eqs. (25) and (26) now. The third line of Eq. (25) does not depend on $H_i(\mathbf{x},t)$ and thus can be calculated directly. It contributes -0.60 μeV to ΔE.

Optimized subtraction scheme.—The master formula (25) allows us to calculate ΔE directly, but it suffers from both the finite-volume effects and the signal-to-noise problem due to the fact that $L_1(\mathbf{x},t_s)$ increases rapidly at large $|\mathbf{x}|$. To solve this difficulty, we define a reduced weight function $L_1^{(r)}(\mathbf{x},t_s)$ as

$$L_1^{(r)}(\mathbf{x},t_s) = L_1(\mathbf{x},t_s) - c_0 L_0(\mathbf{x},t_s) - c_r L_r(\mathbf{x},t_s). \qquad (27)$$

After the replacement of $L_1 \to L_1^r$, the energy shift ΔE is now given by

$$\Delta E = -0.60 + \frac{2m\alpha^2}{\pi M}|\phi_n(0)|^2(c_0 + c_r\langle r_p^2\rangle) + \Delta E_{\mathrm{lat}}, \qquad (28)$$

with ΔE_{lat} computed using the first two lines of Eq. (25) but with L_1 replaced by $L_1^{(r)}$.

Using the least squares method, we determine the coefficients c_0 and c_r by minimizing the following integral

$$I(c_0,c_r) = \int_{R_{\min}}^{R_{\max}} d|\mathbf{x}|(4\pi|\mathbf{x}|^2)|L_1^{(r)}(\mathbf{x},t_s)|^2. \qquad (29)$$

Here we set $t_s = 1$ fm, $R_{\min} = 1$ fm, and $R_{\max} = 3$ fm, and obtain

$$
\begin{aligned}
&\frac{2m\alpha^2}{\pi M}|\phi_n(0)|^2 c_0 = -0.17\ \mu\mathrm{eV}, \\
&\frac{2m\alpha^2}{\pi M}|\phi_n(0)|^2 c_r = -93.72\ \mu\mathrm{eV/fm}^2. \qquad (30)
\end{aligned}
$$

The choice of t_s is made based on the examination of the ground-state dominance. As shown in the Supplemental Material [26], the Fourier transform of $H_1(\mathbf{x},t_s)$ is directly related to the electric form factor $G_E(Q^2)$. To decide $R_{\min}$ and $R_{\max}$, we use the dipole functional form $G_E(Q^2) = 1/(1+Q^2\langle r_p^2\rangle/12)^2$ with $\sqrt{\langle r_p^2\rangle} = 0.85$ fm, and mimic the distribution of $4\pi|\mathbf{x}|^2 L_1(\mathbf{x},t_s)H_1(\mathbf{x},t_s)$ in Fig. 2. The black curve shows that the main contribution comes from the range of 1–3 fm, from which $R_{\min}$ and $R_{\max}$ are decided. After the replacement of $L_1 \to L_1^{(r)}$, the red curve shows

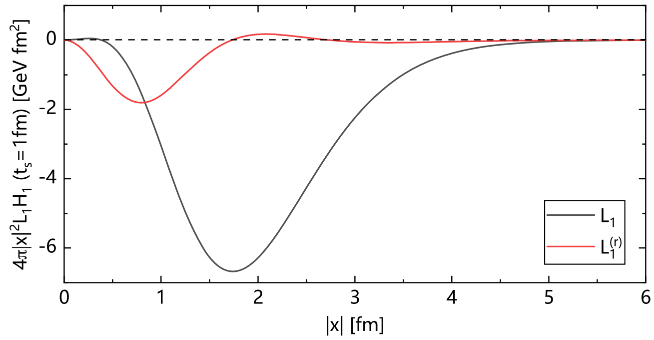

FIG. 2. The distributions of $4\pi|\mathbf{x}|^2 L_1(\mathbf{x},t_s)H_1(\mathbf{x},t_s)$ and $4\pi|\mathbf{x}|^2 L_1^{(r)}(\mathbf{x},t_s)H_1(\mathbf{x},t_s)$ at $t_s = 1$ fm, estimated using the dipole form factor.

that the large-$|\mathbf{x}|$ contribution is significantly reduced, resulting in efficiently suppressed finite-volume effects and statistical noise. Putting Eq. (30) into Eq. (28), ΔE_{TPE} is given by

$$\Delta E_{\mathrm{TPE}} = -\Delta E = 0.77 + 93.72 \cdot \langle r_p^2\rangle - \Delta E_{\mathrm{lat}}. \qquad (31)$$

Numerical results.—To demonstrate the feasibility of the methodology, we use a single gauge ensemble near the physical point, generated by the RBC-UKQCD Collaboration using a $2+1$-flavor domain wall fermion [27]. Ensemble parameters are listed in Table I. We calculate the four-point correlation function $\sum_{\mathbf{x}_f,\mathbf{x}_i}\mathcal{P}\langle\psi_p(\mathbf{x}_f,t_f)J_\mu(x)J_\nu(y)\psi_p^\dagger(\mathbf{x}_i,t_i)\rangle$ using the random field sparsening technique [28,29], with the projection matrix $\mathcal{P} = (1+\gamma_0)/2$ and the proton annihilation operator $\psi_p = \epsilon_{abc}u_a[u_b^T(\mathcal{C}\gamma_5)d_c]$, where u and d are up- and down-quark spinors and $\mathcal{C} = \gamma_0\gamma_2$ is the charge conjugation matrix. The time slices are chosen as $t_i = \min\{t_x,t_y\} - \Delta t_i$ and $t_f = \max\{t_x,t_y\} + \Delta t_f$. The time separation $\Delta t_{i/f}$ should be sufficiently large for the proton ground-state saturation. In practice, we use six sets of $\{\Delta t_i/a, \Delta t_f/a\} = \{1,2\},\{2,1\},\{2,2\},\{2,3\},\{3,2\},\{3,3\}$ to examine the excited-state contamination for the initial or final state and use $t_s/a = 2,3,4,5$ to confirm the ground-state dominance for the intermediate state. The total source-sink time separation ranges from 1.0 to 2.1 fm. We use the local vector current J_μ with the renormalization factor quoted from Ref. [30]. The quark field contractions for the TPE diagrams are shown in Fig. 3, with the first two the connected diagrams and the last three disconnected ones.

TABLE I. Ensemble information. We list the pion mass m_π, the spatial and temporal extents, L and T, the lattice spacing a, and the number of configurations used N_{conf}.

Ensemble	m_π (MeV)	L/a	T/a	a (fm)	N_{conf}
24D	142	24	64	0.1943(8)	131

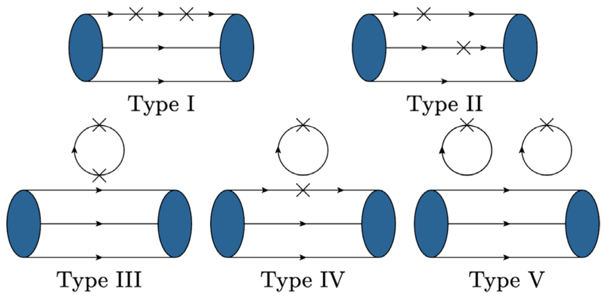

FIG. 3. Five types of quark field contractions. The blob denotes a proton state.

We calculate both connected and disconnected diagrams with only Type IV and V neglected since they vanish in the flavor SU(3) limit.

Using the lattice data at $\{\Delta t_i, \Delta t_f, t_s\} = \{2a, 2a, 4a\}$ as an example, in Fig. 4 we show $\Delta E_{\rm lat}$ as a function of the spatial integral range R. All four contributions to $\Delta E_{\rm lat}$ converge at large R for both connected and disconnected diagrams, suggesting that the finite-volume effects are well under control within current statistical uncertainties. We also examined the R dependence for other sets of $\{\Delta t_i, \Delta t_f, t_s\}$ and the same conclusion holds.

The results of $\Delta E_{\rm lat}$ for different $\{\Delta t_i, \Delta t_f, t_s\}$ are shown in Fig. 5. For the connected part, we find that the result at $\{\Delta t_i, \Delta t_f, t_s\} = \{2a, 2a, 4a\}$ is well consistent with the ones at $\{2a, 2a, 3a\}$ and $\{2a, 2a, 5a\}$. In addition, this result also agrees well with all the data at $\Delta t_{i/f} \geq 2a$. For the disconnected part, the results for various $\{\Delta t_i, \Delta t_f, t_s\}$ are all consistent. The agreement with 0 suggests that the

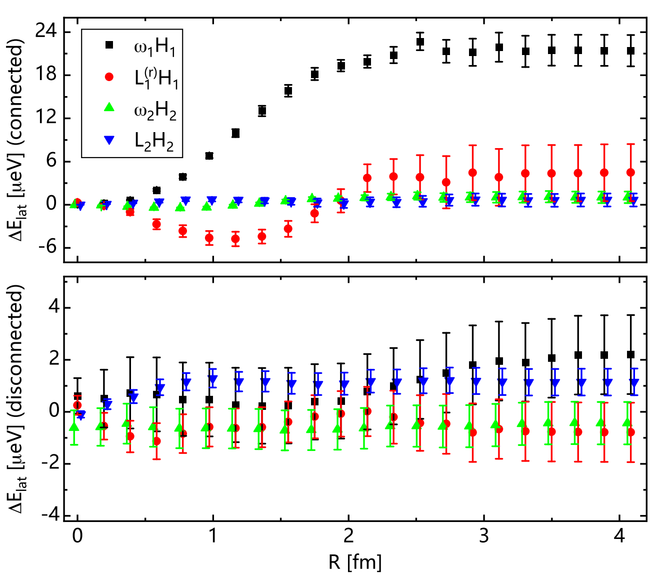

FIG. 4. Results of $\Delta E_{\rm lat}$ as a function of the integral range R at $\{\Delta t_i, \Delta t_f, t_s\} = \{2a, 2a, 4a\}$. The upper and lower panels show the results for the connected and disconnected contribution, respectively. Results from different terms have been slightly shifted for clarity.

disconnected contributions are relatively small. We thus quote $\Delta E_{\rm lat}$ at $\{\Delta t_i, \Delta t_f, t_s\} = \{2a, 2a, 4a\}$ as the final result, and obtain

$$\Delta E_{\rm lat} = \begin{cases} 27.6(4.5)\mu\text{eV}, & \text{connected part}, \\ 2.1(2.1)\mu\text{eV}, & \text{disconnected part}, \\ 29.7(4.9)\mu\text{eV}, & \text{total contribution}. \end{cases} \quad (32)$$

The TPE correction is given by

$$\Delta E_{\rm TPE} = -28.9(4.9)\ \mu\text{eV} + 93.72\ \mu\text{eV}/\text{fm}^2 \cdot \langle r_p^2 \rangle. \quad (33)$$

In both Eqs. (32) and (33) the errors are statistical only.

Combining Eq. (33) with Eq. (1) and comparing the theoretical value with the experimental one, we obtain $\sqrt{\langle r_p^2 \rangle} = 0.84136(65)$ fm, which is consistent with $\sqrt{\langle r_p^2 \rangle} = 0.84087(39)$ fm quoted from μH experiment. On the other hand, if putting the μH value of $\sqrt{\langle r_p^2 \rangle}$ into Eq. (33), we obtain $\Delta E_{\rm TPE} = 37.4(4.9)\ \mu$eV, which agrees with the previous theoretical results ranging from 20 to 50 μeV.

We remark here that this calculation is performed at the nearly physical pion mass but with a relatively coarse lattice spacing $a = 0.1943(8)$ fm. We have used multiple $\{\Delta t_i, \Delta t_f, t_s\}$ to control the excited-state effects and examined the finite-volume effects by studying the R dependence. Thus we expect that the dominant systematic uncertainty arises from the lattice discretization effects. It is our future task to further control these effects using the ensembles with finer lattice spacings.

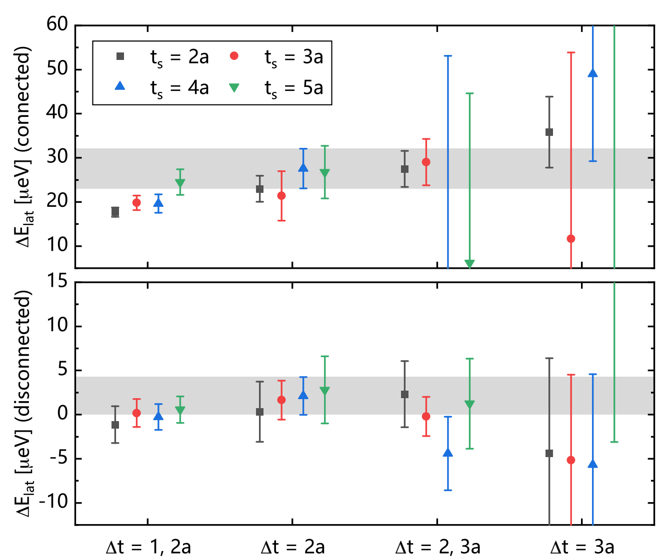

FIG. 5. Results of $\Delta E_{\rm lat}$ for multiple $\{\Delta t_i, \Delta t_f, t_s\}$. The results at different t_s have been shifted horizontally for an easy comparison.

Conclusion.—We developed a method to calculate the TPE correction to the μH Lamb shift using lattice QCD. The methodology includes (i) the derivation of the master formula (25) to remove ir divergence automatically and to compute the ir-finite ΔE using the hadronic functions $H_i(\mathbf{x}, t)$ calculable from lattice QCD and (ii) the design of an optimized subtraction scheme to significantly reduce finite-volume effects and statistical noise. Using the new method, we perform a lattice calculation at $m_\pi = 142$ MeV. It demonstrates that lattice QCD can extend its horizon to study the important quantities relevant for atomic spectroscopy. With both statistical and systematic errors better controlled in the future, lattice studies can help answer more accurately the natural question—how large the proton is.

We gratefully acknowledge many helpful discussions with our colleagues from the RBC-UKQCD Collaborations. We thank M. Gorchtein and C.-Y. Seng for useful communications. X. F., Y. F., and C. F. L. were supported in part by NSFC of China under Grants No. 12125501, No. 12070131001, and No. 12141501, and National Key Research and Development Program of China under No. 2020YFA0406400. L. C. J. acknowledges support by the DOE Office of Science Early Career Award No. DE-SC0021147 and DOE Award No. DE-SC0010339. The calculation is carried out on Tianhe 3 prototype at Chinese National Supercomputer Center in Tianjin. The computation is also performed under the ALCC Program of the U.S. DOE on the Blue Gene/Q (BG/Q) Mira computer at the Argonne Leadership Class Facility, a DOE Office of Science Facility supported under Contract DE-AC02-06CH11357. Computations for this work were carried out in part on facilities of the USQCD Collaboration, which are funded by the Office of Science of the U.S. Department of Energy.

[*]xu.feng@pku.edu.cn
[†]ljin.luchang@gmail.com

[1] R. Pohl *et al.*, Nature (London) **466**, 213 (2010).
[2] A. Antognini *et al.*, Science **339**, 417 (2013).
[3] P. J. Mohr, B. N. Taylor, and D. B. Newell, Rev. Mod. Phys. **84**, 1527 (2012).
[4] N. Bezginov, T. Valdez, M. Horbatsch, A. Marsman, A. C. Vutha, and E. A. Hessels, Science **365**, 1007 (2019).
[5] W. Xiong *et al.*, Nature (London) **575**, 147 (2019).
[6] A. Antognini, F. Kottmann, F. Biraben, P. Indelicato, F. Nez, and R. Pohl, Ann. Phys. (Amsterdam) **331**, 127 (2013).
[7] J. Arrington, P. G. Blunden, and W. Melnitchouk, Prog. Part. Nucl. Phys. **66**, 782 (2011).
[8] K. Pachucki, Phys. Rev. A **60**, 3593 (1999).
[9] A. P. Martynenko, Phys. At. Nucl. **69**, 1309 (2006).
[10] C. E. Carlson and M. Vanderhaeghen, Phys. Rev. A **84**, 020102(R) (2011).
[11] M. Gorchtein, F. J. Llanes-Estrada, and A. P. Szczepaniak, Phys. Rev. A **87**, 052501 (2013).
[12] O. Tomalak, Eur. Phys. J. A **55**, 64 (2019).
[13] J. M. Alarcon, V. Lensky, and V. Pascalutsa, Eur. Phys. J. C **74**, 2852 (2014).
[14] J. M. Alarcón, F. Hagelstein, V. Lensky, and V. Pascalutsa, Phys. Rev. D **102**, 014006 (2020).
[15] D. Nevado and A. Pineda, Phys. Rev. C **77**, 035202 (2008).
[16] M. C. Birse and J. A. McGovern, Eur. Phys. J. A **48**, 120 (2012).
[17] C. Peset and A. Pineda, Eur. Phys. J. A **51**, 156 (2015).
[18] R. J. Hill and G. Paz, Phys. Rev. Lett. **107**, 160402 (2011).
[19] R. J. Hill and G. Paz, Phys. Rev. D **95**, 094017 (2017).
[20] V. Pauk, C. E. Carlson, and M. Vanderhaeghen, Phys. Rev. C **102**, 035201 (2020).
[21] K. Pachucki, Phys. Rev. A **53**, 2092 (1996).
[22] E. Borie, Phys. Rev. A **71**, 032508 (2005).
[23] X. Feng and L. Jin, Phys. Rev. D **100**, 094509 (2019).
[24] J. Gasser, M. Hoferichter, H. Leutwyler, and A. Rusetsky, Eur. Phys. J. C **75**, 375 (2015); **80**, 353(E) (2020).
[25] X. Feng, Y. Fu, and L.-C. Jin, Phys. Rev. D **101**, 051502(R) (2020).
[26] See Supplemental Material at http://link.aps.org/supplemental/10.1103/PhysRevLett.128.172002 for a detailed relation between the hadronic function and the electric form factor.
[27] T. Blum *et al.* (RBC and UKQCD Collaborations), Phys. Rev. D **93**, 074505 (2016).
[28] W. Detmold, D. J. Murphy, A. V. Pochinsky, M. J. Savage, P. E. Shanahan, and M. L. Wagman, Phys. Rev. D **104**, 034502 (2021).
[29] Y. Li, S.-C. Xia, X. Feng, L.-C. Jin, and C. Liu, Phys. Rev. D **103**, 014514 (2021).
[30] T. Blum, P. A. Boyle, N. H. Christ, J. Frison, N. Garron *et al.* (RBC and UKQCD Collaborations), Phys. Rev. D **93**, 074505 (2016).